

PWR2006-88194

THE APPLICATION OF SYSTEMS CFD TO THE DESIGN AND OPTIMIZATION OF HIGH-TEMPERATURE GAS-COOLED NUCLEAR POWER PLANTS

Gideon P. Greyvenstein
Post Graduate School of Nuclear Science and Engineering, North-West University
Potchefstroom, South Africa

ABSTRACT

The basic approach with the design of power plants is to first carry out a thermodynamic cycle analysis and then to vary certain cycle parameters such as the overall pressure ratio in order to determine the optimum or design point condition. One would then proceed to design the different components to match the process conditions.

However, since component design has an impact on overall system performance, one cannot optimize the design of the components in isolation from the rest of the system. This calls for an iterative procedure where one has to move several times between the process and component levels to obtain an optimized integrated solution.

Another problem faced by plant designers is that Computational Fluid Dynamics (CFD) codes that are increasingly used for detailed component design are slow and not well suited for optimization studies. They are not suited at all for the analysis of complete power plants.

Furthermore, the main task of plant designers is not to do design point analyses but to analyze off-design performance, to do uncertainty analyses, to optimize the design and to characterize the dynamic behavior of the system for the purpose of controller design.

An approach that has been used with great success for the design of the power conversion system of the Pebble Bed Modular Reactor (PBMR) is the systems CFD approach. The PBMR is a new High Temperature Gas-cooled Reactor (HTR) that is being developed in South Africa. The PBMR utilizes a direct closed recuperated Brayton cycle. Other cycles are also being investigated including various combined cycles.

Systems CFD codes are based on the network approach and allow one to model the performance of large complex systems in an integrated fashion. Different levels of component models are provided for ranging from lumped models for

components such as pumps to 1D, 2D or even 3D CFD models for components such as complex diffusers, heat exchangers and the pebble bed reactor.

In this paper the systems CFD approach will be discussed including the most important component models.

Various examples of the application of the systems CFD approach in the design of the PBMR plant will be given.

INTRODUCTION

When designing a new power plant one usually starts with a first order cycle analysis to determine the impact of process conditions and cycle lay-out on the performance of the system. The next level of analysis is to improve the accuracy by taking piping losses, compressor and turbine efficiency and secondary flows such as leak or bleed flows into account. Such analyses are known as second order cycle analyses.

With the third level of analysis a simulation model of the system is developed whereby the simple analytical component models employed in the second order analysis are replaced with more advanced implicit or explicit models. System codes usually employ a variety of component models ranging from lookup tables based on component characteristics (as in the case of compressors or turbines) to one-dimensional discretized pipe and heat exchanger models. Third order analyses can either be steady-state or transient and are usually used to investigate the impact of component design or operating conditions on system performance. It can also be used to study the dynamic behavior of the system.

Although third order analysis codes (system codes) utilize more advanced component models compared to second order analyses tools, the component models used in these codes are still not as accurate as can be and this creates a need for fourth level analysis where one would analyze sub-systems such as the boiler, reactor or heat exchangers using state-of-the-art specialized tools such as 3D Computational Fluid Dynamics

(CFD) codes. CFD codes are, however, slow and not well suited for optimization studies. They are not suited at all for the analysis of complete power plants.

In this paper an analysis approach is described, which the authors choose to call the Systems CFD or SCFD approach. This is an extension of third order systems analysis whereby more accurate multi-dimensional CFD models of selected components are embedded into the systems simulation solver. The CFD component models in SCFD codes are usually “tailor made” for the specific component thereby avoiding the overhead of linking a general CFD code with a systems code. This improves ease of use and also leads to faster execution times.

SCFD codes are used to study both system and component performance under varying or transient operating conditions. It is a versatile design tool that can be used for a wide range of tasks such as uncertainty or sensitivity analysis, sizing of component, system optimization, control studies or even the construction of training simulators.

In this paper the application of the SCFD code Flownex for the design of a Pebble Bed type High Temperature Reactor (HTR) nuclear power plant will be discussed. In the first part of the paper a brief description of the HTR power plant will be given. This will be followed by a description of the modeling approach employed in the SCFD code Flownex. In the last part of the paper a number of case studies will be presented.

NOMENCLATURE

b	= dead band
C_t	= turbulent Nusselt number multiplier
D	= diameter or PID controller derivative constant
D_h	= hydraulic diameter of the flow conduit
d	= mass source
\dot{E}	= net energy rate $\dot{Q} - \dot{W}$
f	= Darcy friction factor
h	= enthalpy
I	= controller integral constant or moment of inertia of shaft and all components attached to the shaft
k	= thermal conductivity of the tube side fluid
K	= loss factor of secondary loss components such as bends or inlets
k	= thermal conductivity of tube wall
L	= length of pipe increment
M	= Mach number
m	= mass of fluid in control volume
\dot{m}	= mass flow rate
N	= rotational speed
p	= static pressure
P	= power or controller proportional constant
Pr	= Prandtl number
P_{house}	= house load (electrical)
P_{grid}	= electrical power delivered to grid
\dot{Q}	= heat transfer rate
Q	= volumetric flow rate

R	= gas constant
Re	= Reynolds number
r	= tube radius
t	= time
T	= temperature
V	= velocity
\forall	= volume of control volume
\dot{W}	= work done rate
w	= specific work
x	= controller sensed variable
x_0	= controller set point
y_0	= controller offset
z	= elevation
Δp_0	= $p_{01} - p_{02}$
η	= efficiency
ε	= error
k	= thermal conductivity of the fluid
λ_m	= metal heat transfer coefficient
λ	= surface heat transfer coefficient
ω	= angular speed
θ	= angle between flow direction and vertical
ρ	= density
τ	= time

Subscripts

i	= inside or Node i
f	= fin
gen	= generator
$grid$	= grid
h	= hydraulic
in	= inlet
j	= branch element
$mech$	= mechanical
m	= metal
$switch$	= switching efficiency
out	= outlet
o	= outside
t	= tube
$turbine$	= turbine
0	= stagnation conditions
1	= inlet
2	= outlet

Superscripts

o	= previous time step
τ	= current time step

DESCRIPTION OF PEBBLE BED TYPE HTR POWER PLANT

The power plant that will be considered in this study is a direct two-shaft closed inter-cooled recuperated Brayton cycle

as shown in FIGURE 1. The heat source for the system is a Pebble Bed Reactor [1,2].

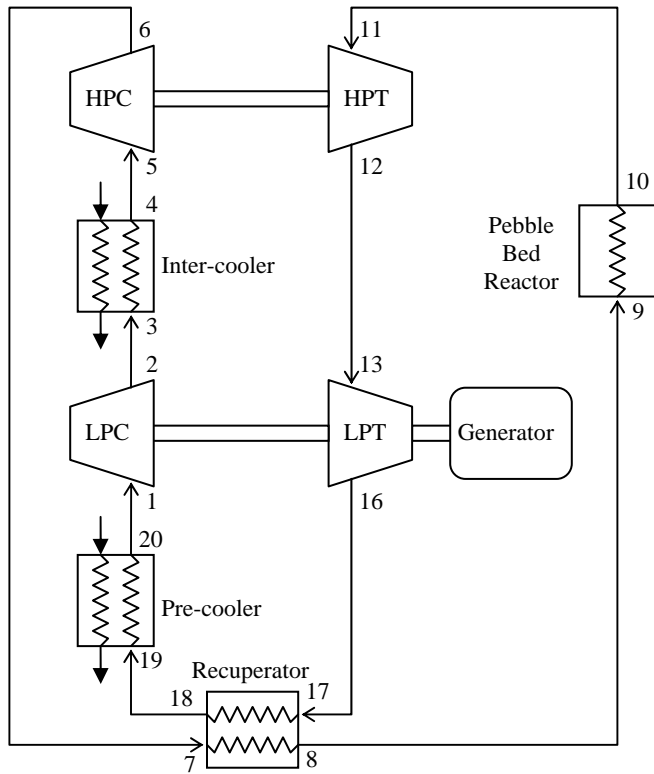


FIGURE 1: Schematic layout of a two-shaft Power Conversion Unit (PCU) for a Pebble Bed type HTR.

Helium enters the Low Pressure Compressor (LPC) at 1 and is then compressed to state 2. From 3 to 4 the helium is cooled in the intercooler where after it is re-compressed in the High Pressure Compressor (HPC) to state 6. The helium is then pre-heated in the recuperator (7-8) and then further heated to the maximum cycle temperature in the reactor (9-10). The hot high pressure helium is expanded to an intermediate pressure in the High Pressure Turbine (HPT) (11-12), which drives the HPC. It is then further expanded in the Low Pressure Turbine (LPT) (13-16), which drives both the LPC and the generator. After the LPT the still hot helium is passed through the recuperator (17-18) where it is cooled to state 18 while at the same time pre-heating the helium leaving the HPC before it enters the reactor. The helium is then further cooled in the pre-cooler to state 20 before entering the LPC.

PLANT PARAMETERS

A second order cycle analysis was performed using a range of pressure ratios to determine the optimum overall pressure ratio. The input parameters used in this analysis is summarized in TABLE 1.

The reason why the pressure drop relationship $\Delta p = C_2 Q$ is used for the recuperator as apposed to $\Delta p = C_1 \rho Q^2$ for the pre-cooler and inter-cooler is that the flow in the recuperator is

laminar while the flow in the pre-cooler and inter-cooler is turbulent.

The second order cycle analysis yielded an optimum overall pressure ratio of approximately 3.0. Assuming the pressure ratios of the two compressors to be the same the pressure ratio of each compressor will therefore be $\sqrt{3} = 1.732$.

Parameter	Value
Maximum cycle pressure	7000 kPa
Lowest cycle temperature (T_1, T_4, T_5, T_{20})	24 °C
Maximum cycle temperature (T_{10}, T_{11})	900 °C
Heat released in the reactor	260 MW
Compressor isentropic efficiency	88 %
Turbine isentropic efficiency	91 %
Turbo machine mechanical efficiency	99 %
Recuperator effectiveness	96 %
Compressor and turbine exit velocities	135 m/s
Compressor and turbine exit losses	$\Delta p_0 = 0.3 \times \frac{1}{2} \rho V^2$
Pipe velocities	
Sections 4-5 & 20-1	50 m/s
Section 8-9, 10-11 & 18-19	80 m/s
Pipe losses	
Primary losses	$0.1 \times \frac{1}{2} \rho V^2$
Secondary losses	$0.4 \times \frac{1}{2} \rho V^2$
Total losses	$0.5 \times \frac{1}{2} \rho V^2$
Pipe inside surface roughness	30 μm
Leak flows	
From 6 to 13	1.25 %
From 2 to 17	3.75 %
Reactor pressure loss	$\Delta p_0 = 21.827 \times \rho Q^2$
Pre-cooler pressure loss	$\Delta p_0 = 0.05684 \times \rho Q^2$
Inter-cooler pressure loss	$\Delta p_0 = 0.05684 \times \rho Q^2$
Recuperator hot side pressure loss	$\Delta p_0 = 24.047 \times \rho Q^2$
Recuperator cold side pressure loss	$\Delta p_0 = 36.657 \times \rho Q^2$

TABLE 1: Plant parameters.

Normally Flownex is used to simulate the performance of a given system. In this example the second order analysis is used to determine near optimum process conditions for the system as a whole, which are then used to determine the component designs. With the component designs fixed the behavior of the system is investigated under both steady-state and transient operating conditions.

In the next section the Flownex modeling approach will be discussed where after the component models used in the modeling of the example system shown in FIGURE 1 will be discussed.

SYSTEMS CFD APPROACH TO THE MODELING OF THERMAL-FLUID SYSTEMS

In the SCFD approach a thermal-fluid system is represented by a network of nodes and elements as shown in FIGURE 2. Elements are components such as pipe increments,

valves, compressors or heat exchangers, while nodes are the end points of elements. Nodes can also be used to represent reservoirs with specified volumes.

Elements can be connected in any arbitrary way at common nodes to form a network. Flownex solves the momentum equation in each element and the continuity and energy equation at each node. This gives Flownex a pseudo CFD capability, which enables it to predict complex phenomena such as pressure and temperature waves in pipes and buoyancy effects in packed beds.

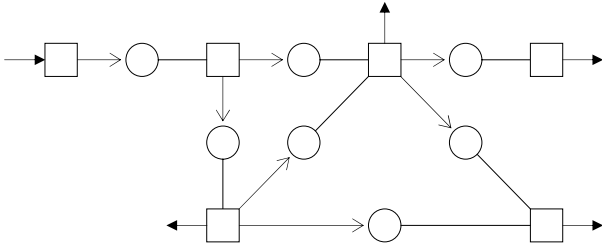


FIGURE 2: Discretization of a thermal-fluid system into a network of nodes and elements.

An important feature of the network approach is that elements such as pipes, heat exchangers and the reactor, although depicted on the systems level as single elements or pairs of elements, can be discretized into either sub-networks or multidimensional CFD regions as explained later.

Flownex can also handle 2D conductive heat transfer structures connected to flow elements. The discretization of these elements is beyond the scope of this paper.

Numerical approach for solution of the flow, pressure and temperature fields. The equations that govern the solution of mass flows, pressures and temperatures are the continuity, momentum and energy equations. Consider a general node i with J branches as shown in FIGURE 3.

The continuity equation for node i can be expressed as:

$$\mathbf{V}_i \frac{\partial \rho_i}{\partial t} = \sum_{j=1}^J \rho_j Q_j s_j + d_i \quad (1)$$

where s_j is the ‘sign’ of element j with $s_j = 1$ if the positive flow direction of element j is from node j to node i and $s_j = -1$ if the positive flow direction is from node i to node j .

The momentum equation for element j can be written in the following general form:

$$f(\rho_j, Q_j) + \frac{\rho_j \Delta x}{A} \frac{\partial Q_j}{\partial t} + s_j (p_i - p_j) = 0 \quad (2)$$

where Δx is the length of the element and A is the average cross sectional area.

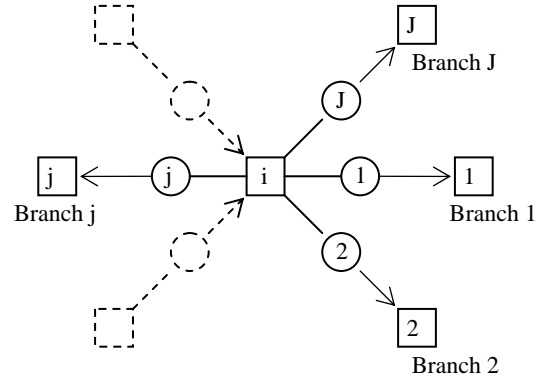


FIGURE 3: General node with neighboring nodes connected through branch elements.

The energy conservation equation for node i is given by:

$$\frac{\partial(m_i h_i)}{\partial t} - \mathbf{V}_i \frac{\partial p_i}{\partial t} = \sum_{in,j} [s_j \dot{m}_j (h_j + gz_j) + \dot{E}_j] + d_i^+ (h_{amb} + gz_i) + (h_i + gz_i) \left(\sum_{out,j} s_j \dot{m}_j - d_i^- \right) + \dot{E}_i \quad (3)$$

Eqs. (1) to (3) are simultaneously solved with the Implicit Pressure Correction Method (IPCM), described elsewhere [3-5].

Calculation of turbo machine shaft speed. The speed of a turbo machine shaft is governed by the following equation:

$$\frac{d\omega}{dt} = \frac{P}{I\omega} \quad (4)$$

The net shaft power is calculated as

$$P = \eta_{mech} \sum P_{turbine} - \sum P_{compressor} - (P_{grid} / \eta_{switch} + P_{house}) / \eta_{gen} \quad (5)$$

Equation (4) is solved numerically at each time step for all shafts in the system.

PID Controller. A PID controller senses one variable and adjusts the value of another variable according to the following relationship:

$$y = y_0 + P\varepsilon + I \int_0^t \varepsilon d\tau + D \frac{d\varepsilon}{d\tau} \quad (6)$$

The error is defined as follows:

$$\begin{aligned} \varepsilon &= x_0 + b/2 - x & \text{if } x > x_0 + b/2 \\ \varepsilon &= x_0 - b/2 - x & \text{if } x < x_0 - b/2 \\ \varepsilon &= 0 & \text{if } x_0 - b/2 \leq x \leq x_0 + b/2 \end{aligned} \quad (7)$$

In discretized form, as implemented in the solution algorithm, Eq. (6) becomes:

$$y = y_0 + P\varepsilon + I \sum_{\tau=1}^{\tau=t} \varepsilon^\tau \Delta t + D(\varepsilon - \varepsilon^o) / \Delta t \quad (8)$$

COMPONENT MODELS

In this section the different component models used in the Flownex analysis of the system will be briefly discussed.

Restrictors with loss coefficient. Compressor and turbine exit losses are modeled with Flownex's RL element. RL elements are used for the following sections in FIGURE 1: 2-3, 6-7, 12-13 and 16-17.

The pressure drop through an RL element is given by

$$\Delta p_0 = c_L p_{01} \left(1 - \frac{p_s}{p_{01}} \right) \quad (9)$$

while the mass flow rate is given by

$$\dot{m} = c_D \rho V A \quad (10)$$

Using gas dynamics relationships for an ideal gas, the Mach number in the throat can be expressed in terms of p_s / p_{01} as:

$$M = \sqrt{\frac{2}{\gamma-1} \left[\left(1 - \frac{\Delta p_0}{c_L p_{01}} \right)^{\frac{1-\gamma}{\gamma}} - 1 \right]} \quad (11)$$

Using Eqs. (9) to (11) together with values of \dot{m} and ρ obtained from the second order cycle analysis, the throat diameters of the different RL elements were determined as follows:

Section	d [m]
2-3	0.4761
6-7	0.3602
12-13	0.6814
16-17	0.9019

Pipes. The following sections in FIGURE 1 represent pipes: 4-5, 8-9, 10-11, 18-19, and 20-1.

The pressure drop for incompressible flow through pipes is modeled as

$$\Delta p_0 = \left(\frac{fL}{D} + \sum K \right) \frac{1}{2} \rho V^2 + \rho g L \cos \theta + \rho L \frac{dV}{dt} \quad (12)$$

For compressible flows the pressure drop is given by

$$\frac{p}{p_0} \Delta p_0 = \left(\frac{fL}{D} + \sum K \right) \frac{1}{2} \gamma p M^2 + \rho g L \cos \theta + \rho L \frac{dV}{dt} \quad (13)$$

In TABLE 1 the primary losses of all pipe sections is specified as $0.1 \times (\frac{1}{2} \rho V^2)$ while the secondary losses is specified as $0.4 \times (\frac{1}{2} \rho V^2)$. The primary loss is defined as

$$\Delta p_{0,p} = \left(f \frac{L}{d} \right) \frac{1}{2} \rho V^2$$

while the secondary loss is defined as

$$\Delta p_{0,s} = \sum K \frac{1}{2} \rho V^2$$

K is the loss coefficient of components such as bends and valves. This implies that $f \frac{L}{d} = 0.1$ and $\sum K = 0.4$ for all pipes.

For turbulent flow the Darcy friction factor in (12) is calculated with the Swamee-Jain equation [7], which is given by

$$f_t = 0.25 \left\{ \log \left[\left(\frac{e}{3.7D} \right) + 5.74 \text{Re}^{-0.9} \right] \right\}^{-2} \quad (14)$$

where e is the inside surface roughness and Re is the Reynolds number.

For laminar flow ($\text{Re} \leq 2300$) the friction factor is given by

$$f_l = \frac{64}{\text{Re}} \quad (15)$$

For transitional flow ($2300 \leq \text{Re} \leq 5000$) Flownex interpolates between f_t and f_l .

Using values of \dot{m} , ρ and f obtained from the second order cycle analysis the lengths and diameters of the different diffusers were determined as follows:

Section	d [m]	L[m]
4-5	0.6929	6.506
8-9	0.6632	6.059
10-11	0.8284	7.539
18-19	0.8657	8.254
20-1	0.9275	8.983

Orifices Use to Model the Leak Flows. Two leak flows, not shown in FIGURE 1, are taken into consideration. One is between positions 6 and 13 and one between positions 2 and 17. These flows are modeled with Flownex's RD (Restrictor with Discharge Coefficient) element.

The pressure drop for compressible flow through RD elements is given by

$$\Delta p_0 = p_{01} \left(1 - \frac{p_s}{p_{01}} \right) \quad (16)$$

where p_s is the static pressure in the throat of the restrictor.

Using gas dynamics relationships for an ideal gas, the Mach number in the throat can be expressed in terms of p_s / p_{01} :

$$M = \sqrt{\frac{2}{\gamma-1} \left[\left(1 - \frac{\Delta p_0}{p_{01}} \right)^{\frac{1-\gamma}{\gamma}} - 1 \right]} \quad (17)$$

where γ = ratio of specific heats.

The mass flow rate through RD elements is given by

$$\dot{m} = c_D \rho V A \quad (18)$$

With the mass flows and pressures known from the second order cycle analysis, Flownex's designer capability was used to determine the orifice diameters. These are as follows:

Section	d [m]
6-13	0.021283
2-17	0.043358

The discharge coefficient, c_D , of both restrictors is assumed to be 1.0.

Pre-cooler and intercooler. The pre-cooler is modeled with Flownex's FTX (Finned Tube Heat Exchanger) element. FTX heat exchangers consist of rows of finned tubes spaced along the circumference of a cylindrical pressure vessel.

The liquid is normally on the tube side while the gas is on the shell side. The liquid normally flows radially inwards while the gas flows radially outwards as shown in FIGURE 4.

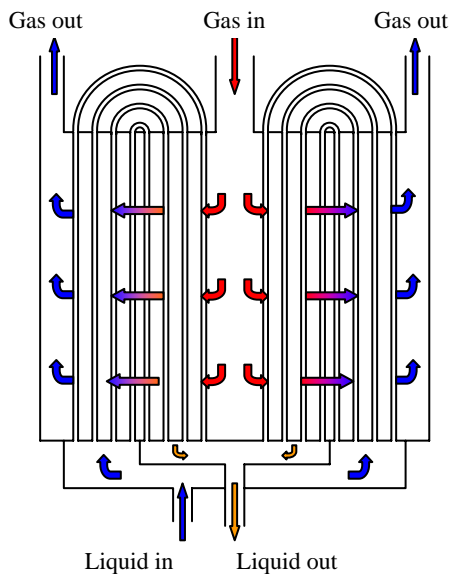


FIGURE 4: Flownex's finned tube heat exchanger.

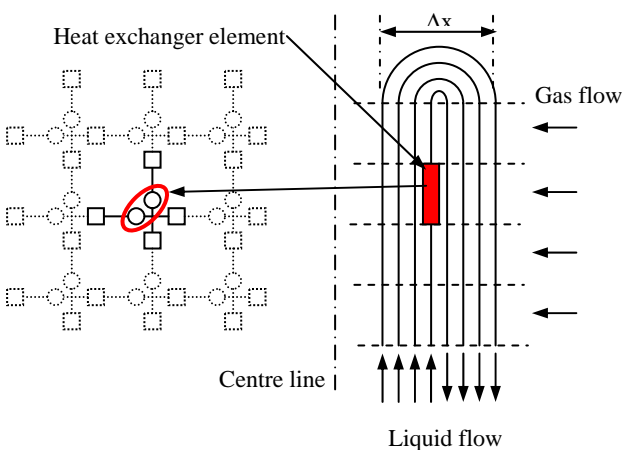


FIGURE 5: Discretization of finned tube heat exchanger.

Pressure drop. The pressure drop on the tube side is given by

$$\Delta p_0 = \left(\frac{fL}{D} + K_{in} + K_{out} \right) \frac{1}{2} \rho V^2 + \rho L \frac{dV}{dt} \quad (19)$$

while the pressure drop on the shell side is given by

$$\Delta p_0 = \frac{4fL}{D_h} \frac{1}{2} \rho V^2 + \rho L \frac{dV}{dt} \quad (20)$$

where

f = friction factor given as function of Reynolds number as part of the input data, and

V = maximum velocity based on the minimum flow area.

The hydraulic diameter is calculated as

$$D_h = \frac{4LA_{min}}{A_o} \quad (21)$$

where

A_{min} = minimum flow area on the shell side and

A_o = shell side heat transfer area.

Heat transfer. Consider a heat exchanger increment as shown in FIGURE 6.

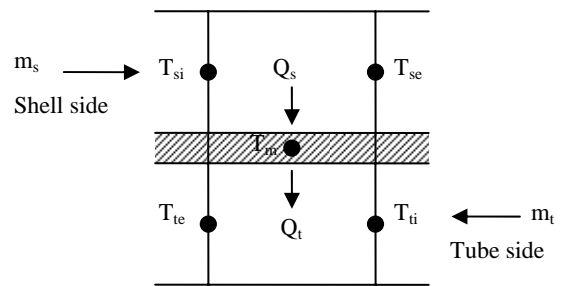


FIGURE 6: Notation used to describe heat transfer in a heat exchanger element.

In the above figure the subscripts denote the following:

- t = tube side,
- s = shell side,
- m = metal,
- si = shell side inlet,
- se = shell side outlet,
- ti = tube side inlet and
- te = tube side outlet.

The shell side heat transfer is calculated as

$$Q_s = A_s U_s \left[\frac{1}{2} (T_{si} + T_{se}) - T_m \right] \quad (22)$$

where A_s is the shell side heat transfer area and U_s is the shell side effective heat transfer coefficient, which is given by

$$U_s = \left(\frac{1}{\eta_{fs} \lambda_s} + \frac{0.5}{\lambda_m} \right)^{-1} \quad (23)$$

where

- η_{fs} = fin efficiency on the shell side,
- λ_t = shell side surface heat transfer coefficient, and
- λ_m = metal coefficient.

The shell side surface heat transfer coefficient is determined from a user specified curve which gives $St Pr^{2/3}$ as a function of the Reynolds number where St is the Standton number and Pr is the Prandtl number.

The metal coefficient is given by

$$\lambda_m = \frac{2\pi kL}{A_s \ln(r_o/r_i)} \quad (24)$$

If there are no extended surfaces (fins) on the tube side we can write that

$$2\pi L = A_t / r_i \quad (25)$$

where A_t is the tube side heat transfer area.

Substitution of (25) into (24) leads to

$$\lambda_m = \frac{A_t}{A_s} \frac{k}{r_i \ln(r_o/r_i)} \quad (26)$$

The tube side heat transfer is given by

$$Q_t = A_s U_t [T_m - \frac{1}{2}(T_{ti} + T_{te})] \quad (27)$$

where U_t is the tube side effective heat transfer coefficient, which is given by

$$U_t = \left(\frac{A_s}{A_t} \frac{1}{\eta_{ft} \lambda_t} + \frac{0.5}{\lambda_m} \right)^{-1} \quad (28)$$

where

- η_{ft} = fin efficiency on the tube side surface and
- λ_t = tube side surface heat transfer coefficient.

The tube side heat transfer coefficient is calculated with the Dittus-Boelter equation, which is given by

$$\frac{\lambda_t D_t}{k} = 0.023 Re^{0.8} Pr^n \quad (29)$$

where n is 0.4 for heating and 0.3 for cooling.

Recuperator. The recuperator is modeled with Flownex's recuperator element. This is a counter flow or parallel heat exchanger (depending on the flow direction of the two streams) divided into a number of increments in the flow direction as shown in FIGURE 7.

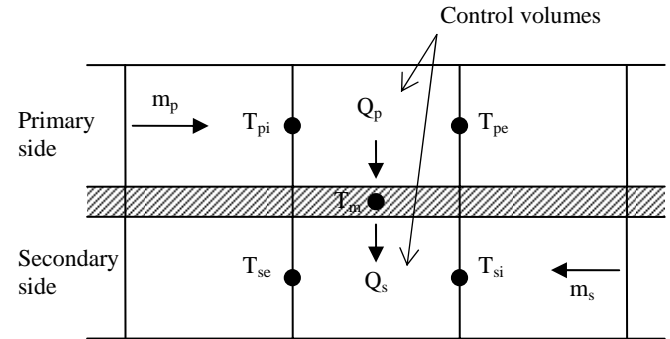


FIGURE 7: Discretization of counter/parallel flow heat exchanger.

The subscripts in FIGURE 7 denote the following:

- p = primary side,
- s = secondary side,
- m = metal,
- pi = primary side control volume inlet and
- pe = primary side control volume outlet.
- si = secondary control volume side inlet,
- se = secondary control volume side outlet,

Pressure drop. The pressure drop through a flow conduit increment is given by

$$\Delta p_0 = \frac{fL}{D} \frac{1}{2} \rho V^2 + \rho L \frac{dV}{dt} \quad (30)$$

The friction factor is calculated as follows:

$$Re > 5000: f_t = F_t 0.25 \left\{ \log \left[\left(\frac{e}{3.7D} \right) + 5.74 Re^{-0.9} \right] \right\}^{-2} \quad (31)$$

$$Re < 2300: f_t = \frac{F_t 64}{Re} \quad (32)$$

where F_t is the turbulent friction multiplier and F_l is the laminar friction multiplier. These multipliers are user specified and are introduced to provide for non-circular cross-sectional channel shapes.

For $2300 \leq Re \leq 5000$ Flownex interpolates between f_t and f_l .

Heat transfer. Consider the control volumes shown in FIGURE 7. The heat transfer rate to the primary and secondary side fluid control volumes is calculated as follows

$$Q_p = A_p U_p \left[\frac{1}{2} (T_{pi} + T_{pe}) - T_m \right] \quad (33)$$

and

$$Q_s = A_s U_s \left[T_m - \frac{1}{2} (T_{si} + T_{se}) \right] \quad (34)$$

The heat transfer coefficients are given by

$$U_p = \left(\frac{1}{\eta_{fp} \lambda_p} + \frac{A_p \Delta x}{A_m 2k} \right)^{-1} \quad (35)$$

and

$$U_s = \left(\frac{1}{\eta_{fs} \lambda_s} + \frac{A_s \Delta x}{A_m 2k} \right)^{-1} \quad (36)$$

where

- A_p = heat transfer area on the primary side
- A_s = heat transfer area on the secondary side and
- A_m = heat transfer area in the middle of wall separating the primary side from the secondary side.

For the recuperator model it is assumed that $A_m = A_s$ and that $\eta_{fp} = \eta_{fs} = 1$.

The surface heat transfer coefficients are calculated as follows:

$$\text{Re} > 5000: \quad \lambda_t = \frac{k C_f (0.023) \text{Re}^{0.8} \text{Pr}^n}{D_h} \quad (37)$$

$$\text{Re} < 2300: \quad \lambda_t = \frac{k \text{Nu}_t}{D_h} \quad (38)$$

For $2300 \leq \text{Re} \leq 5000$ Flownex interpolates between λ_t and λ_t .

Compressors. Compressor performance is usually expressed in terms of the pressure ratio (PR) and efficiency as functions of non-dimensional mass flow and non-dimensional speed.

The pressure ratio of a compressor is defined as the ratio of the total pressure at the outlet (p_{02}) to the total pressure at the inlet (p_{01}). Therefore

$$PR = \frac{p_{02}}{p_{01}} \quad (39)$$

The efficiency is defined as

$$\eta = \frac{c_p T_{01} (PR^{(\gamma-1)/\gamma} - 1)}{w} \quad (40)$$

The non-dimensional mass flow is defined as

$$NDM = \frac{\dot{m} \sqrt{RT_{01}}}{p_{01} D^2} \quad (41)$$

whereas non-dimensional speed is defined as

$$NDS = \frac{ND}{\sqrt{RT_{01}}} \quad (42)$$

For a given machine working with only one type of gas both R and D will be constant so that it is somewhat more convenient to express the pressure ratio and efficiency as functions of

corrected mass flow (CMF) and corrected speed (CS), which are defined as

$$CMF = \frac{\dot{m} \sqrt{T_{01}}}{P_{01}} \quad (43)$$

and

$$CS = \frac{N}{\sqrt{T_{01}}} \quad (44)$$

The following speed values for the two compressors are assumed:

HP Compressor: 10800 RPM

LP Compressor: 3600 RPM

The operating point values of CMF and CS are calculated using the above speed values together with the values of mass flow, pressure and temperature obtained from the second order cycle analysis. These values together with the pressure ratios and efficiencies are summarized in the following table.

Parameter	Units	LP Compressor	HP Compressor
CMF	[kg/s]*sqrt[K]/Bar	94.443	52.719
CS	[rev/s]/sqrt[K]	3.481	10.441
PR	ratio	1.732	1.732
Efficiency	fraction	0.88	0.88

TABLE 2: Operating points of compressors.

The pressure ratio and efficiency characteristics of the LP compressor are shown in FIGURE 8 and FIGURE 9. These characteristics were obtained by scaling the characteristics of a typical axial flow machine to give the required values of pressure ratio and efficiency at the operating point. The characteristics of the HPC have a similar shape but scaled to the right operating conditions.

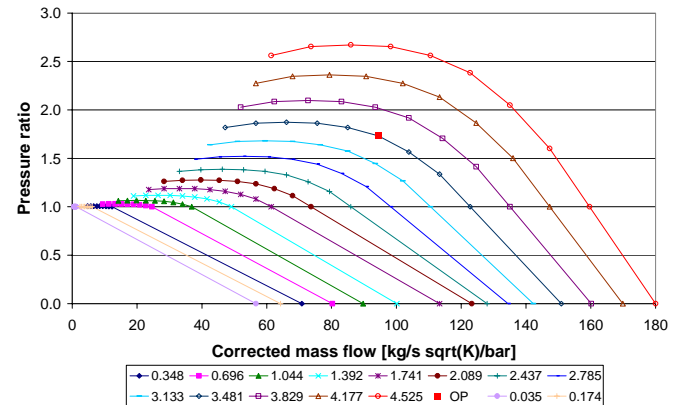


FIGURE 8: LPC pressure ratio characteristics.

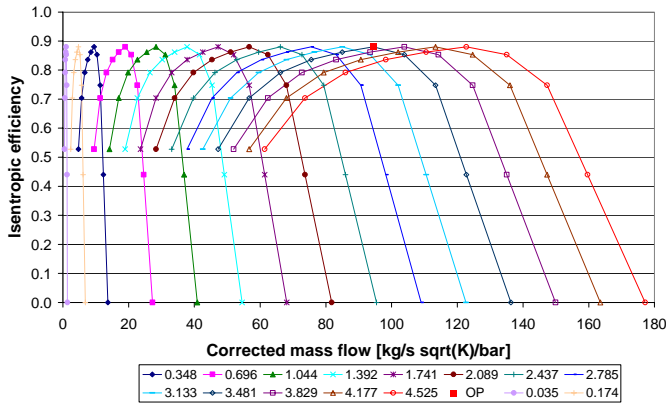


FIGURE 9: LPC efficiency characteristics.

Turbines. Turbine performance is also expressed in terms of pressure ratio (PR) and efficiency as functions of corrected mass flow and corrected speed.

The pressure ratio of a turbine is defined as the ratio of the total pressure at the inlet (p_{01}) to the total pressure at the outlet (p_{02}). Therefore

$$PR = \frac{p_{01}}{p_{02}} \quad (45)$$

The efficiency is defined as

$$\eta = \frac{w}{c_p T_{01} (1 - PR^{(1-\gamma)/\gamma})} \quad (46)$$

where w is the work done by the fluid and γ is the ratio of specific heats.

The corrected mass flow (CMF) and corrected speed (CS) are defined as follows:

$$CMF = \frac{\dot{m} \sqrt{T_{01}}}{p_{01}} \quad (47)$$

and

$$CS = \frac{N}{\sqrt{T_{01}}} \quad (48)$$

The following speed values are assumed for the two turbines:

HP Turbine: 10800 RPM

LP Turbine: 3600 RPM

The values of CMF and CS at the operating point are calculated using the above speed values together with the values of mass flow, pressure and temperature obtained from the second order cycle analysis. These values together with the pressure ratios and efficiencies are summarized in the following table.

Parameter	Units	LP Turbine	HP Turbine
CMF	[kg/s]*sqrt[K]/Bar	72.581	60.644
CS	[rev/s]/sqrt[K]	1.8265	5.2553
PR	ratio	2.3722	1.230
Efficiency	fraction	0.91	0.91

TABLE 3: Operating points of turbines.

The pressure ratio and efficiency characteristics of the LP turbine are shown in FIGURE 10 and FIGURE 11. These characteristics were obtained by scaling the characteristics of a typical axial flow machine to give the required values of PR and efficiency at the operating point. The characteristics of the HPT have a similar shape but scaled to the right operating conditions.

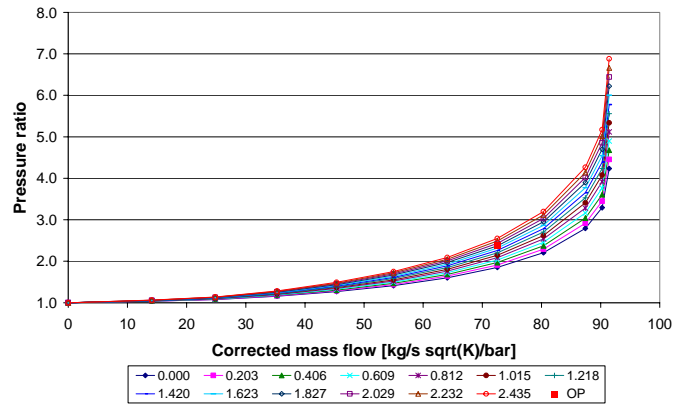


FIGURE 10: LPT pressure ratio characteristics.

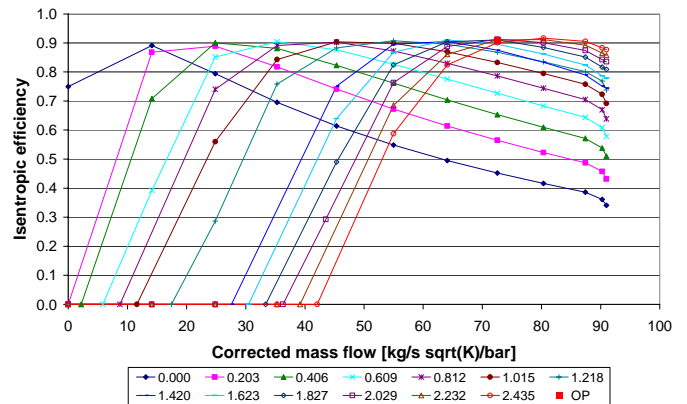


FIGURE 11: LPT efficiency characteristics.

Pebble Bed Reactor. Flownex uses a distributed model equivalent to a 2D CFD method to solve the flow, pressure and temperature distribution inside the pebble bed reactor [8]. Consider a staggered CFD grid in the r-z plane of a cylindrical co-ordinate system as shown in FIGURE 12.

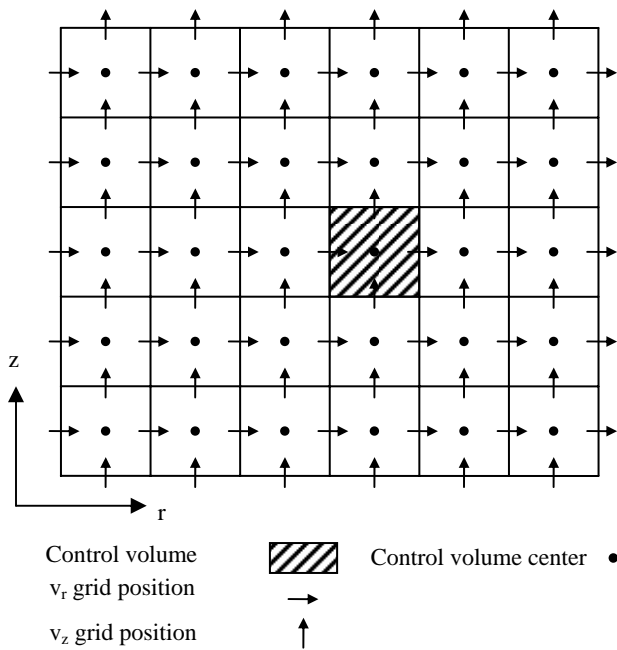


FIGURE 12: Staggered CFD grid of the flow domain inside the reactor.

FIGURE 13 shows the network representation of the staggered CFD grid with nodes representing the control volume centres and the elements representing the convective fluxes across control volume boundaries.

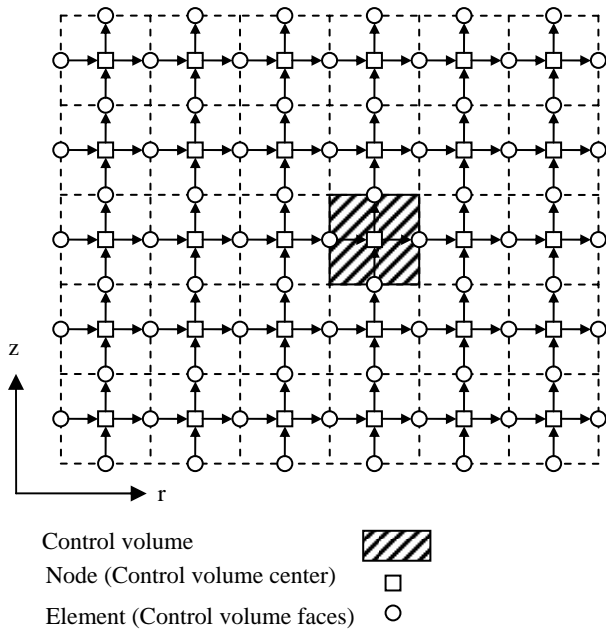


FIGURE 13: Flownex network representation of staggered CFD grid.

Eqs. (1) and (3) are applied to the nodes inside the reactor whereas an appropriate form of Eq. (2), applicable to flow through a porous medium, is applied to the elements.

The fission heat released inside the pebbles is modeled with a point kinetics neutronics model [9]. The heat transfer inside the pebbles, heat transfer between the pebbles and heat transfer from the pebble surface to the gas is modeled through an additional network superimposed on the gas flow network as shown in FIGURE 14.

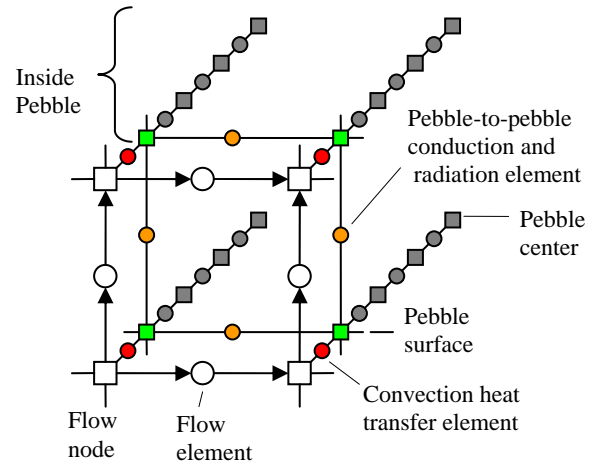


FIGURE 14: Network for calculating heat transfer inside the pebbles, between pebbles and between pebbles and gas.

A more detailed description of the reactor model can be found elsewhere [6].

SIMULATIONS

The Flownex network of the system is shown in FIGURE 15.

In this section three cases will be considered namely the steady-state operation at design condition, startup, and load rejection at full load.

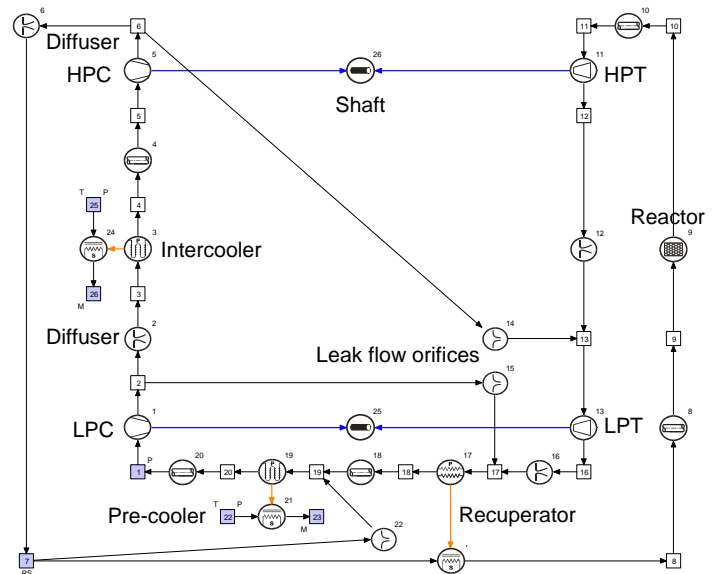


FIGURE 15: Flownex network of the direct two-shaft closed inter-cooled recuperated Brayton cycle PBMR power plant.

Steady-state Operation at Design Conditions. The only boundary condition of the gas loop is the fixed pressure of 2333.3 kPa at Node 1. The temperature boundary conditions of 22 °C are set at Nodes 22 and 25, which are the water side inlets of the pre-cooler and intercooler respectively. These temperatures affect the helium temperatures through the pre-cooler and intercooler.

The initial speed of the high-pressure turbo charger is intentionally set as 7200 rpm (as apposed to the known value of 10800 rpm) to demonstrate the code’s shaft balancing capability. By specifying an approximate shaft speed and then selecting the appropriate option Flownex will automatically determine the shaft speed at which the power delivered by the turbine exactly matches the power required by the compressor and any additional loads.

The reactor exit temperature is fixed at 900°C. Alternatively one can specify a fixed heat transfer.

TABLE 4 compares some Flownex results with the second order cycle analysis results obtained with EES¹. The agreement between the two sets of results is excellent.

Parameter	Units	Flownex	EES
Mass flow rate	kg/s	127.8	127.8
Net work	MW	126.2	126.4
Reactor heat	MW	259.8	260.0
Thermal efficiency	%	48.6	48.6
Maximum cycle pressure	kPa	6967.5	6968.5
HP turbo unit shaft speed	rpm	10793	10800
Pre-cooler heat	MW	78.1	78.3
Intercooler heat	MW	53.0	53.0
Recuperator heat	MW	240.2	240.1
LP compressor power	MW	55.1	55.1
HP compressor power	MW	52.9	53.0

TABLE 4: Comparison between Flownex results and second order cycle analysis results obtained with EES.

Startup. The initial condition for the startup simulation is the steady-state solution for a shaft speed of 1 rps for both the HP and LP shafts. The boundary condition for the initial steady-state simulation is a fixed pressure of 3610 kPa at Node 1 and a reactor outlet temperature of 900 °C. The pressure boundary condition at Node 1 was determined through trial and error to give a pressure of 2333.3 kPa after the system has reached full power design point operation. At the start of the transient simulation the fixed pressure condition at Node 1 is released while the total mass in the system is kept constant.

A controller senses the speed of the LPC/LPT shaft and then adjusts the power of the generator load on the shaft in such a way that the generator initially acts as a motor that drives the shaft and then changing over to a generator load that

approaches the design point value as the speed of the shaft approaches the design speed.

FIGURE 16 to FIGURE 20 show the variation of pressures, temperatures, mass flows, shaft speeds and generator power during startup.

As can be seen from FIGURE 17 the temperature at the inlet of the power turbine (Node 16) increases above 900 °C during startup. Since the power turbine is usually designed for a lower inlet temperature this may be a problem.

FIGURE 21 shows the variation of maximum fuel temperature during start-up. As can be seen the maximum fuel temperature does not exceed the maximum allowable value of 1600 °C. This is a good example of the information that can be obtained from a systems CFD simulation. To obtain the same kind of information without the systems CFD approach would require quite more time and effort.

FIGURE 22 and FIGURE 23 show the locus plot of the HPC and LPC operating points during startup. While the operating point of the HPC stays well clear of the surge line, the operating point of the LPC at low speeds falls within the surge region. This is undesirable and it is an issue that warrants further investigation. What this however demonstrates is that one can not select component characteristics with only steady-state operation in mind. One has to take the impact of component characteristics on system performance during operational transients also into account. This is a task where systems CFD analysis is very helpful.

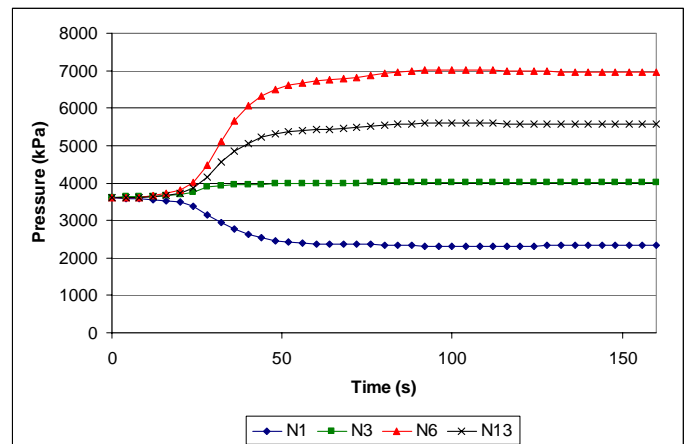


FIGURE 16: Variation of pressures during startup (N = Node).

¹ Engineering Equation Solver, www.fChart.com

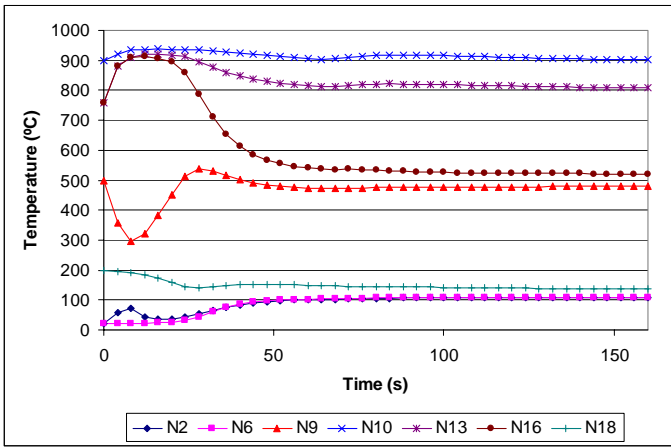


FIGURE 17: Variation of temperatures during startup.

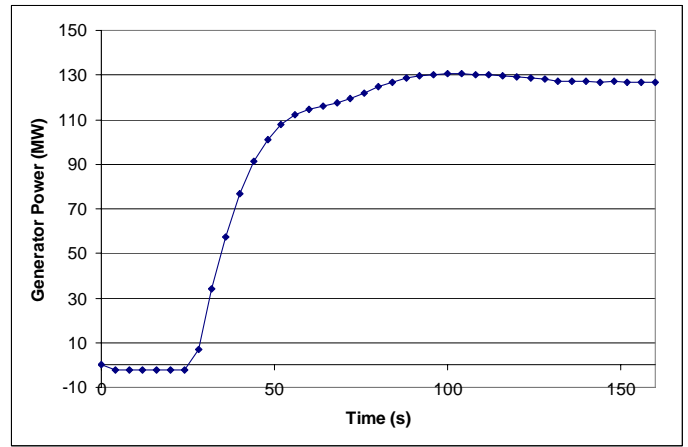


FIGURE 20: Variation of generator power during startup.

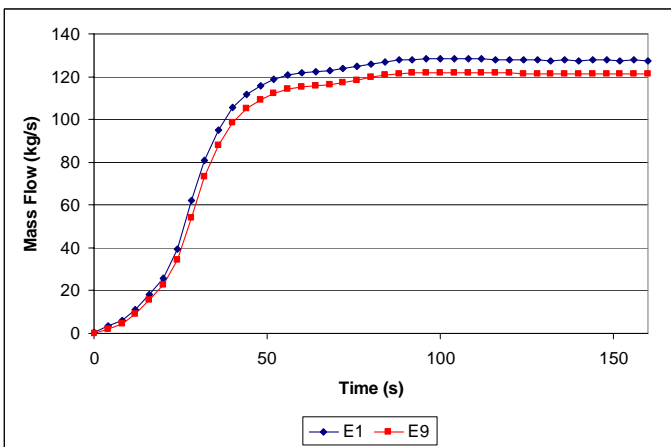


FIGURE 18: Variation of mass flows during startup ($E =$ Element).

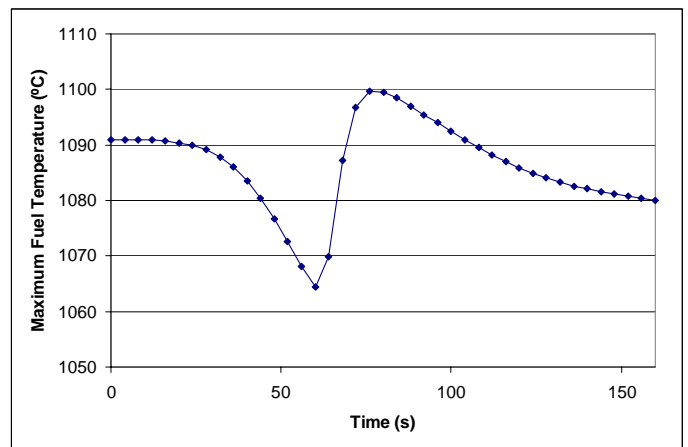


FIGURE 21: Maximum fuel temperature during startup.

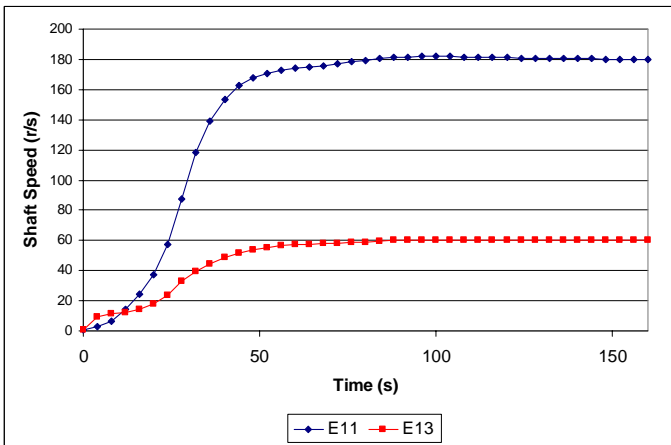


FIGURE 19: Variation of shaft speeds during startup ($E =$ Element).

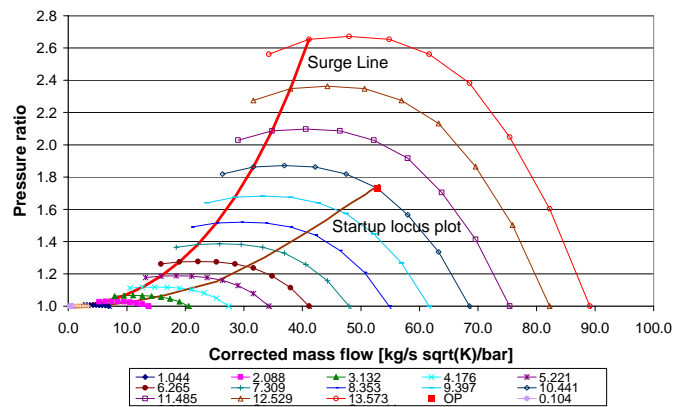


FIGURE 22: Locus plot of HPC operating point during startup.

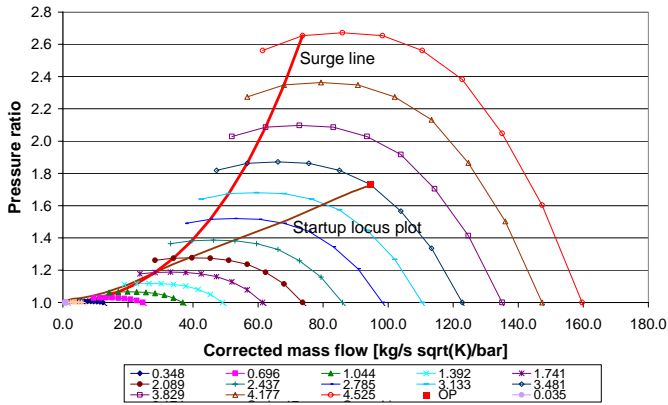


FIGURE 23: Locus plot of LPC operating point during startup.

Load Rejection. In this example the situation is considered where the generator load is suddenly dropped to zero from a full load condition. A controller senses the speed of the LPC/LPT shaft and then adjusts the opening of the by-pass valve (Element 22) in an effort to keep the speed of the shaft constant at 60 rps.

FIGURE 24 to FIGURE 28 show the variation of pressures, temperatures, mass flows, shaft speeds and control valve opening during the load rejection transient.

As can be seen from FIGURE 25 the temperature to the inlet of the reactor increases about 500 °C during the load rejection transient. This may be a problem that requires some modifications.

From FIGURE 27 it can be seen that the speed of the LPT stays nearly constant during the transient, which illustrates the effectiveness of the control mechanism to control the generator speed during sudden variations in the generator load.

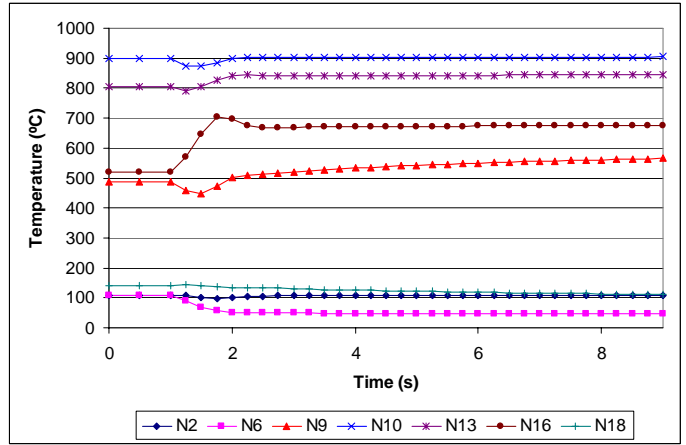


FIGURE 25: Variation of temperatures during load rejection.

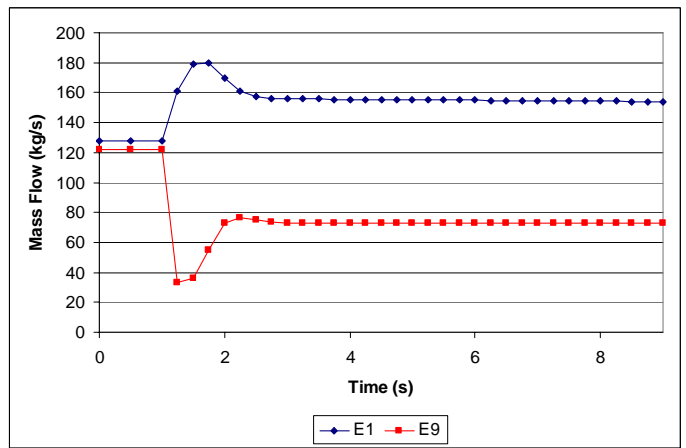


FIGURE 26: Variation of mass flows during load rejection.

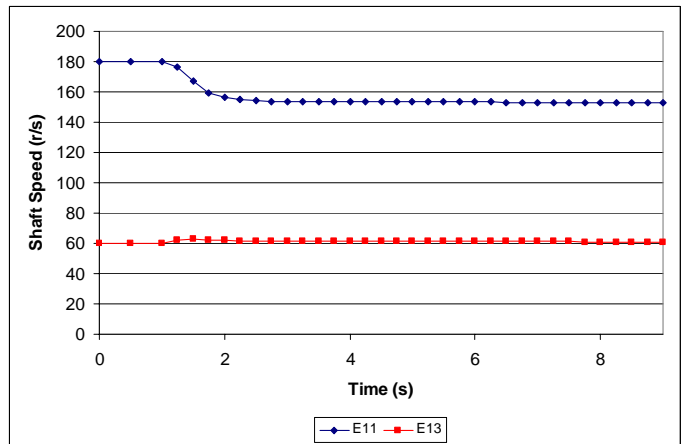


FIGURE 27: Variation of shaft speeds during load rejection.

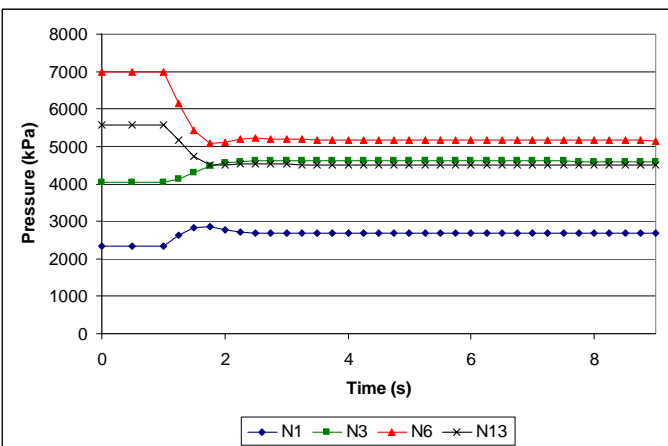


FIGURE 24: Variation of pressures during load rejection.

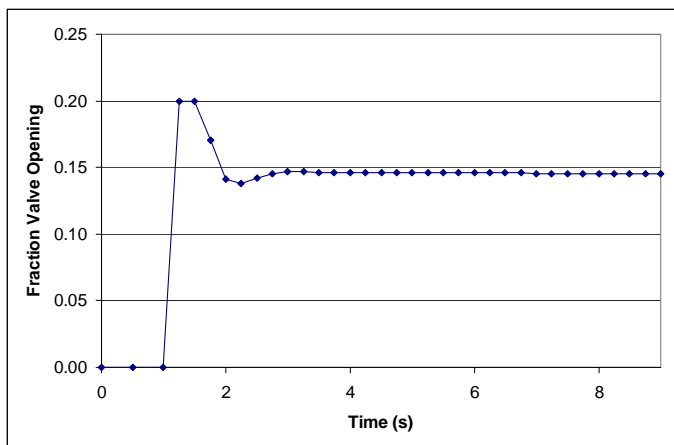


FIGURE 28: Variation of valve opening during load rejection.

This case demonstrates how a SCFD code can be used to test control strategies.

CONCLUSIONS

In this paper the modeling of a Pebble Bed type High Temperature Reactor power plant with the aid of the systems CFD code Flownex is discussed. The different component models are discussed together with a brief description of the overall solution algorithm. The main advantage of the systems CFD approach is the excellent balance between accuracy and speed. It allows one to obtain detail information of component and systems performance during both steady-state and transient operation. It is a valuable design tool that finds application in a wide range of design activities such as systems lay-out, sizing of components, sensitivity analyses, optimization studies and dynamic characterization. In this paper it was demonstrated how detail information on critical parameters such as turbine and reactor inlet temperatures, maximum fuel temperature and compressor surge margin during operational transients can be obtained. It was also demonstrated how a SCFD code can be used to test control strategies.

ACKNOWLEDGEMENTS

The author wishes to thank PBMR (Pty) Ltd. whose financial support made this work possible as well as M-Tech Industrial (Pty) Ltd., developers of the Flownex software.

REFERENCES

- [1] PBMR (Pty) Ltd. Reactor Safety Analysis Report of the South-African Pebble-Bed Modular Reactor (PBMR), Rev. E, Centurion, South Africa.
- [2] PBMR Website. www.pbmr.co.za.
- [3] Greyvenstein, G. P., and Laurie, D. P., 2002, "A segregated CFD approach to pipe network analysis", *Int. J. of Numerical Methods in Engineering*, 37, pp 3685 - 3705.
- [4] Greyvenstein, G.P., 2002, "An implicit method for the analysis of transient flows in pipe networks", *Int. J. of Numerical Methods in Engineering*, 53(5), pp 1127-1143.

- [5] Greyvenstein G. P., Van Ravenswaay J. P., and Rousseau P. G., 2002, "Dynamic modelling of heat, mass and momentum transfer in the pebble bed modular reactor", 1st Int. Conf. On Heat Transfer, Fluid Mechanics and Thermodynamics (HEFAT 2002), Kruger Park, South Africa.

- [6] Du Toit, C.G., Rousseau, P.G., Greyvenstein, G.P., and Landman, W.A., 2005, "A systems CFD model of a packed bed high temperature gas-cooled nuclear reactor", *Int. J. of Thermal Sciences* 45, pp 70–85.

- [7] Swamee, P.K., and Jain, A.K., 1976, "Explicit Equations for Pipe-Flow Problems", *J. Hydraulic Div. Proc. ASCE*, pp. 657-664.

- [8] Patankar, S.V., 1980, *Numerical Heat Transfer and Fluid Flow*. McGraw Hill, New York.

- [9] Rousseau, P.G., and Greyvenstein, G.P., 2003, "One-dimensional reactor model for the integrated simulation of the PBMR power plant", *Proc. 1st Int. Conf. on Heat Transfer, Fluid Mechanics and Thermodynamics*, Kruger Park, South Africa, April 8-10, 2002.